

HIGH-G (>20,000g) INERTIAL SHOCK SURVIVABILITY OF EPITAXIALLY ENCAPSULATED SILICON MEMS DEVICES

David B. Heinz, Vu A. Hong, Yushi Yang, Chae-Hyuck Ahn and Thomas W. Kenny
Stanford University, Stanford, California, USA

ABSTRACT

In this work, we demonstrate both high-frequency (1.12 MHz) MEMS tuning fork resonators and lower frequency (39kHz) MEMS test devices capable of withstanding large magnitude inertial shocks. These devices reliably continue to function after the application of repeated inertial shocks in excess of 20,000g. The device performance, and the robust, pure silicon encapsulated environment are both preserved. Detailed before/after analysis and high-speed real time measurements confirm the functionality of the devices. High frequency, single anchored devices display no measureable change in properties, and even low frequency devices have high survival rates and only small changes in surface adhesion.

INTRODUCTION

As compared to macro-scale mechanical devices and sensors, MEMS devices have numerous intrinsic benefits with regards to isolation from the environmental error interference. In particular, the small characteristic size and low mass contribute to high natural resonant frequencies and reduced interaction with macro-scale dynamics. These features, along with the cost, performance and robustness of MEMS sensors has enabled their use in a variety of demanding environments, such as mobile electronics [1], and automotive sensors [2].

While MEMS devices have already been used successfully in many challenging applications, there are still significant limitations with regards to high-g inertial shocks and high vibration amplitude [3]. Military and aerospace [4] applications, among many others, typically require devices to withstand high vibration and shock amplitudes. Typical high-performance MEMS devices become susceptible to failure modes including mechanical wear, stiction [3], fracture of delicate suspension and anchoring structures [5], material fatigue [6] or disruption of hermetic packaging [7] under these demanding conditions.

Numerous efforts have previously been made to design and fabricate MEMS sensors that are well suited to harsh environments. Simple design modifications rely upon strengthening released structures and increasing spring stiffness, but these approaches sacrifice sensitivity and other important performance metrics. Extremely hard materials such as silicon carbide [8] are often employed for harsh environment applications. These materials can have improved mechanical properties, but they are costly and difficult to process. Active cancellation of vibrations has also been explored as an environmental isolation strategy [9], but this increases system complexity, and may not be well suited to high-g shocks.

Traditional silicon MEMS may possibly be adapted to these conditions as well. Silicon has proved to be a useful mechanical material [10] with stable, predictable properties. Under hermetic encapsulation, it has been demonstrated to have high strength and no fatigue [11]. Previous work has demonstrated structures that reduce the intensity of surface collisions to prevent damage [12]. These features suggest that there is potential for silicon MEMS in high-g applications.

EXPERIMENT DESIGN

A custom built test apparatus was constructed to allow the instrumented and repeatable application of high-g shocks up to 50,000g. A series of MEMS test structures was selected to study the effect of these high-g shocks on several key elements of MEMS device performance. State of the art packaging technology allowed for clear and repeatable results, despite the highly demanding testing process.

Device Fabrication Process

Test devices were designed and fabricated in a hermetic, epitaxial silicon encapsulation process. This process yields pure single crystal silicon devices in an ultra-clean, vacuum environment. This process has been described extensively elsewhere [13], but has several important benefits related to high-g testing and shock survival.

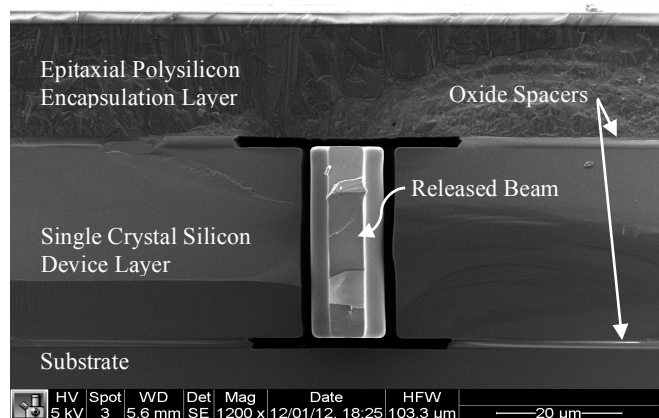


Figure 1 - A single released beam fabricated within the robust, epitaxial encapsulation process

The robust monolithic encapsulation, shown in figure 1, allows the devices to be mounted directly to the equipment required for high-g testing. No special handling precautions or isolation (e.g. vacuum chambers, or electrical noise isolation) is required to maintain device performance. In addition, the device layer within the encapsulation consists of pure, fatigue-free, single crystal silicon. The absence of native oxides, polymer anti-stiction coatings, chemical getters, and other materials greatly simplifies analysis, and increases chances of device survival.

Test Device Design

Two distinct types of devices were designed, fabricated, and tested to ensure the high-g test results are relevant to a wide array of device configurations and performance metrics. The devices are tuning fork resonators and stiction test structures. Schematics of these devices are shown in figure 2.

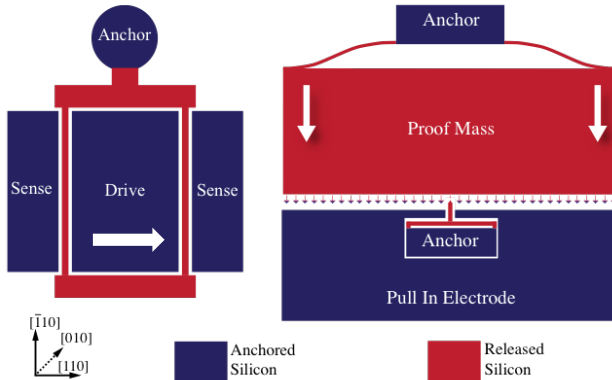


Figure 2 - Top view schematic of tuning fork (left) and stiction test structure (right) used for high-g testing. Arrows indicate respective direction of applied test acceleration.

The double ended tuning fork (DETF) device is prototypical of many MEMS resonators. Similar structures have been used as timing references, strain gauges, thermometers, and other such devices. The design used for this test has a resonant frequency of $\sim 1.12\text{MHz}$, and a quality factor above 10k, when driven electrostatically. Previous studies have shown the frequency and quality factor to be extremely stable. Other features of relevance are the single anchor point, which prevents substrate stress coupling, and the uniform 1um gaps between the free-standing resonator and the fixed electrodes. These devices allow for careful examination of the effect of high-g shocks on frequency stability and resonator performance.

The stiction test structures have also been studied extensively to determine the nature of the silicon-silicon surface adhesion in this encapsulated environment [12]. The devices are designed to have many features in common with a generic inertial sensor, such as resonant frequency around 39kHz, a substantial proof mass, and parallel plate electrostatic sensing and actuation. A bump stop limits the contact area, and prevents shorting between the proof mass and sense electrodes. The sensing and actuation allows the released proof mass to be pulled-in to and detached from contact with the bump stop to measure the stiction force. This configuration presents the opportunity to study survival of a less stiff, higher displacement device, and changes in surface adhesion resulting from high-g impacts.

High-G Experiment Procedure

A custom setup was designed and fabricated to allow high-g shocks to be applied in a repeatable and measurable manner. The setup, shown in figure 3, consists of a cart mounted on frictionless linear air bearings, and an effectively immovable (50kg) block of plain steel.

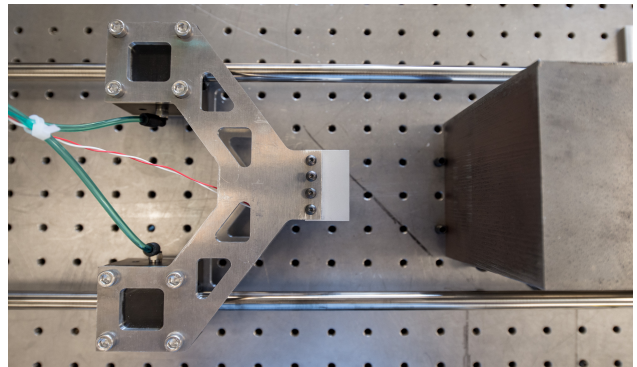


Figure 3 – Custom built high-g shock test setup

The cart is given an initial velocity and then allowed to strike the steel block. The cart is constructed of high-strength aluminum, and has machined features to minimize squeeze film damping upon impact with the block. The sudden deceleration of the cart can reach peaks up to 50,000g, with durations upwards of 30 μs , as recorded by a reference accelerometer (PCB PiezoTronics 350D02).

The device-under-test is mounted at the tip of a printed circuit board (PCB), in a rigid, leadless ceramic chip carrier. The PCB is mounted in a pre-stressed configuration to ensure the device-under-test receives the same acceleration as the metal housing. This assumption is verified using high-speed videography and image processing. The mounting PCB has connectors to allow for limited electrical transduction throughout the test procedure.

RESULTS AND DISCUSSION

Several of each of the devices shown in figure 2 were carefully characterized in several methods to determine the resilience against high-g shocks. The results for each type of device are presented in the following sections.

Tuning Fork Frequency Stability

Several tuning forks were tested to determine the stability of the resonant behavior. This was done by taking measurements of the frequency response in a temperature stabilized oven before and after application of high-g shocks.

An example acceleration measurement from a high-g shock used in DETF testing is shown in figure 4.

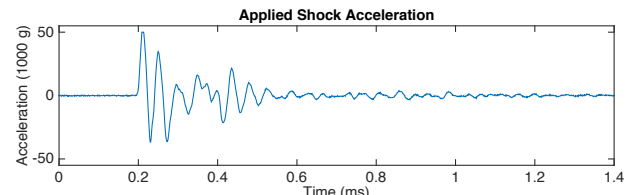


Figure 4 - Applied high-g shock, measured by reference accelerometer

Despite the application of repeated high-g shocks, the devices remain fully functional with stable characteristics. The exterior of the epitaxially encapsulated package is visually unaffected, as shown in figure 5.

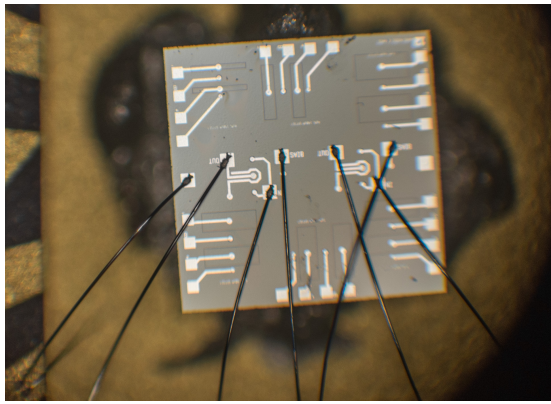


Figure 5 - Optical microscope image of a hermetic device package after repeated shock testing

Careful characterization of the open-loop resonant properties of the DETF show no significant changes. Frequency response data collected before and after shock testing is presented in figure 6.

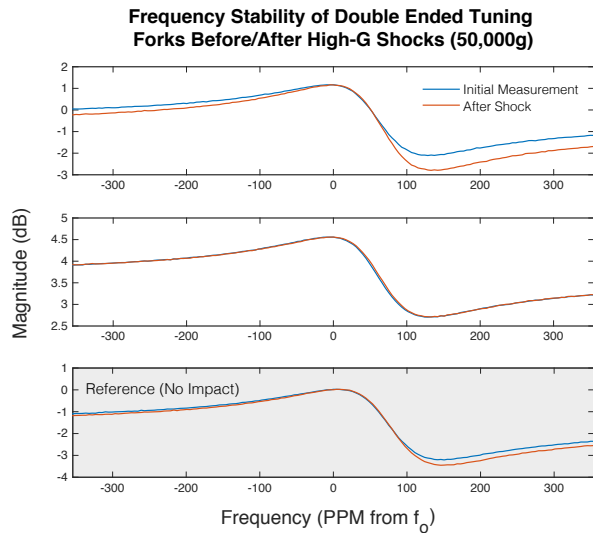


Figure 6 - Frequency responses for two DETF devices before and after shock, and a third reference DETF. Frequency normalized to initial freq. for each device ($f_0 \approx 1.121\text{MHz}$)

There is some small change in the anti-peak (caused by parasitic feedthrough) evident in the frequency spectrum of one of the devices, but, crucially, there is no measureable change in resonant frequency at the PPM level for any tuning fork device, and the quality factor appears to remain stable. The change in feedthrough could result from displacement of the unshielded wirebonds.

Simulation indicates that impacts above 40,000g should cause the free end of the tuning fork to collide with the fixed electrodes, as shown in figure 7. This suggests that though the resonator contacts the fixed surroundings, the silicon in the contact area stays below the fracture strength, and no permanent modifications occur.

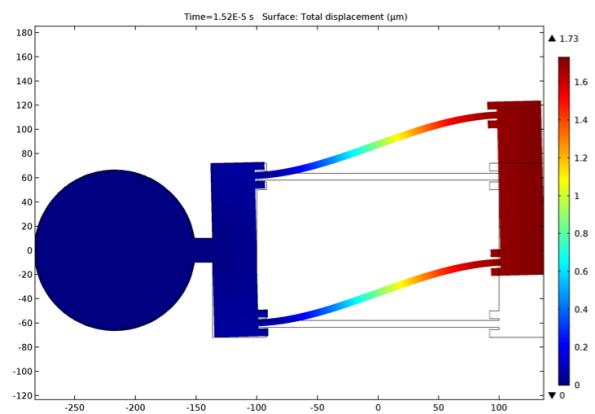


Figure 7 - Finite element simulation of DETF at 45,000g. The fabricated device has a gap of $\sim 1.5\mu\text{m}$ to the fixed electrodes

The result demonstrates that high frequency resonators and timing references fabricated in the epitaxial encapsulation process are well suited to high shock applications. The devices tested here had no specific design features to enable shock survival, and yet reliably continued to function after shock testing.

Stiction Test Structures Surface Adhesion

A pull-in and release test was performed before and after several impacts to measure the effect of high-g shocks on surface adhesion. The results of this measurement for a typical device are shown in figure 8.

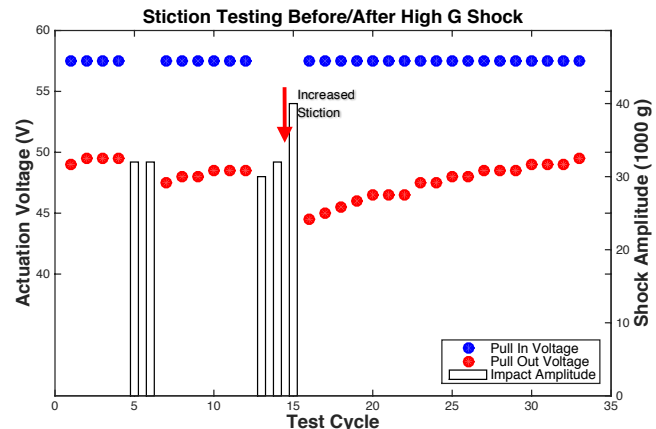


Figure 8 - Results of electrostatic surface adhesion testing before and after several high-g shocks

This measurement indicates that there is a slight increase in the stiction force following high-g impacts, and that the increase is larger for correspondingly larger impacts. This can be seen in the decrease in pull-out/detachment force that occurs after a high-g impact, as this is a proxy measurement for the adhesion force. While the tuning fork resonators appeared to be completely unchanged, there are some measureable surface adhesion changes to these devices. This result is likely due to the larger collision forces caused by the substantial proof mass, and more compliant springs in this device design.

The non-contact behavior of the released structure, however, appears to remain stable, as demonstrated by the constant pull-in voltage. This parameter is determined by the suspension springs and geometry of the electrodes. This suggests that only a very small modification to the contact area occurs, and the bulk device performance is unchanged.

Stiction Test Structure In-Situ Testing

Though all of the test structures reliably continued to operate after a high-g test, it is still interesting to gain insight into the dynamics of the proof mass during the course of the testing. In order to achieve this, a DC bias was applied to the proof mass and bump stop, and the pull-in electrode was connected to virtual ground on a transimpedance amplifier, as shown in figure 9. This allows the amplification and measurement of the motional current generated during the impact. A small DC bias was chosen to prevent electrostatic pull-in from significantly impacting the dynamics.

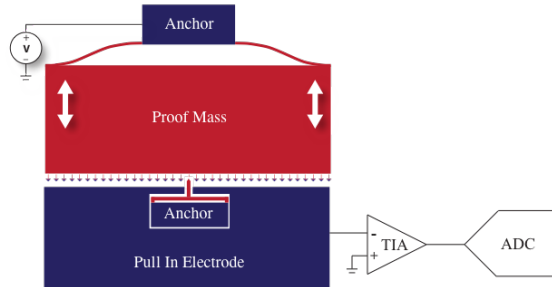


Figure 9 - Test setup for real-time in-situ testing

High-g tests were performed on the test structures while collecting data at up to 500MS/s. The result, shown in figure 10, show the motion of the proof mass.

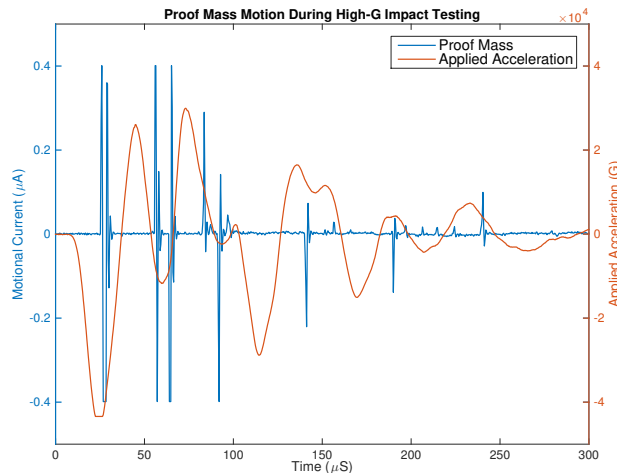


Figure 10 - Measurement result showing the proof mass motion during the application of 40,000g shock

The in-situ measurement demonstrates that proof mass is repeatedly colliding with the over travel stops, and rebounding in the opposite direction during the peaks of applied acceleration. The current peaks are artificially sharpened by the jump discontinuity in capacitance that

occurs when the proof mass makes or breaks electrical contact with the bump stop.

CONCLUSIONS

The high-g shock test results are very promising for use of these devices under harsh environment conditions. Precise high-frequency resonators remain stable to the PPM level despite high-g shocks, and even devices with a significant proof mass have high survival rates with modest modification of the surface adhesion. These test results indicate that the epitaxial encapsulation process provides a robust, high-stability environment, which enables reliable mechanical performance for high-g shock applications.

ACKNOWLEDGEMENTS

This work was supported by DARPA grant N66001-12-1-4260, "Precision Navigation and Timing program (PNT)," managed by Dr. R. Lutwak. Work was performed in part at the Stanford Nanofabrication Facility, supported by the National Science Foundation under Grant ECS-9731293. Substantial support of this project is also provided by the Robert Bosch Research and Technology Center, and we acknowledge many useful technical discussions with Gary Yama and Gary O'Brien.

REFERENCES

- [1] J. Gubbi, et al., "Internet of Things (IoT): A vision, architectural elements, and future directions," *Future Generation Computer Systems*, vol. 29, (2013)
- [2] C. Akar, et al., "Environmentally Robust MEMS Vibratory Gyroscopes for Automotive Applications," *IEEE Sensors*, vol. 9, no. 12, (2009)
- [3] T.G. Brown, "Harsh Military Environments and MEMS Devices," *Proc. of IEEE Sensors*, (2003)
- [4] H. Shea, "Reliability of MEMS for space applications," *Proc. of SPIE*, vol. 6111, (2003)
- [5] Woon, Sang Yon. *Vibration Isolation and Shock Protection for MEMS*. N.p.: ProQuest U of Michigan, 2009.
- [6] P.O. Theillet, et al., "Fatigue rates of monocrystalline silicon thin films in harsh environments: Influence of stress amplitude, relative humidity, and temperature," *Applied Physics Letters*, vol. 94, (2009)
- [7] P. Lall, et al., "Failure-Envelope Approach to Modeling Shock and Vibration Survivability of Electronic and MEMS Packaging", *IEEE Trans. Comp. Pack. Tech.*, Vol. 31 (2008)
- [8] M. Mehrgany, et al., "Silicon Carbide MEMS for Harsh Environments," *Proc. IEEE*, vol. 86, No. 8 (1998)
- [9] Y. Meyer, et al., "Active isolation of electronic micro-components with piezoelectrically transduced silicon MEMS devices," *Smart Mater. Struct.*, vol. 16 (2007)
- [10] K. Petersen, "Silicon as a Mechanical Material," *Proc. IEEE*, vol. 70, no. 5, (1982)
- [11] V.A. Hong, et al., "Fatigue Experiments on Single Crystal Silicon in an Oxygen-Free Environment," *JMEMS*, vol. 24, no. 2, (2015)
- [12] D.B. Heinz, et al., "Experimental Investigation Into Stiction Forces and Dynamic Mechanical Anti-Stiction Solutions in Ultra-Clean Encapsulated MEMS Devices," *JMEMS*, vol. 25, no. 3, (2016).
- [13] R.N. Candler, et al., "Single wafer encapsulation of MEMS Devices," *IEEE Trans. Adv. Pack*, vol. 26, (2003)